Multispectral VIS-NIR whole-body imaging: Equipment and skin cancer patient data

Janis Spigulis*[a], Uldis Rubins[a], Edgars Kviesis-Kipge[a], Marta Skrastina[a], Jekaterina Tihomirova[a], Anda Apine[b], Egija Vasilishina[b]

[a] Institute of Atomic Physics and Spectroscopy, University of Latvia, FST, Jelgava Street 3, Riga, LV-1004, Latvia;
[b] Oncology Center of Latvia, Riga East University Hospital, Hipokrata Street 4, Riga, LV-1038, Latvia

ABSTRACT

To ensure high spectral selectivity of whole-body skin diagnostics and early cancer screening, a prototype device for skin multispectral imaging at narrow 450/520/638/850/940 nm spectral bands has been developed and clinically validated. Skin images were captured by a high-resolution color camera with removed infrared cut-off filter under spectrally specific multi-laser or 940 nm LED illumination. The camera, surrounded by two side-emitting optical fiber spirals coupled with visible RGB laser and 850 nm near-infrared laser, could be moved up and down, while imaging of any diseased skin area was ensured by positioning the patient in front of camera. The system was clinically validated in Oncology Center of Latvia on 60 patients diagnosed with basal cell carcinoma, malignant melanoma or skin lesions suspected of malignancy. Analysis of clinical data confirmed promising potential of NIR imaging for skin cancer detection and screening. Details of the equipment design and image analysis procedure, as well as the results of patient measurements are presented.

Keywords: remote skin diagnostics, whole-body imaging, multi-laser illumination, NIR imaging, skin cancer.

1. INTRODUCTION

Remote whole-body imaging systems recently have gained attention in dermatology as efficient tools for skin cancer detection and monitoring [1]. Contrary to the classic investigations focused on a single lesion examined by a dermoscope or other specialized imager, such systems collect numerous high-resolution photographs of the whole body – either from all sides simultaneously, or from one side with appropriate patient's body position changes. Along with capability of multiple lesion detection in a single procedure, this allows comparing images acquired during dynamic monitoring to identify the lesion growth indicative of potential malignancies. Several advanced (and correspondingly expensive) whole body imaging systems are on the market - see [2,3] as examples. The available systems use broadband white light sources that function well for uniform body illumination; still, the captured color photos under such illumination lack the possibility of extracting characteristic spectral features of the skin lesions for more precise diagnostics.

Spectral images taken within specific narrow wavelength bands provide more information on the biochemical content and structure of skin malformations. Multispectral imaging of single skin malformations is a powerful tool for skin cancer detection and screening [4-8]. However, the procedure may be very time-consuming if the patient has numerous suspicious skin lesions to be examined - e.g. tens of them on the back. Remote and fast multispectral analysis of the whole-body skin or selected large skin areas could be a better option for mass screening of skin cancer.

To avoid motion artefacts in images related to different spectral regions, snapshot capturing of the whole spectral image data set is helpful. Recently a technique called "snapshot multi-spectral-line imaging" or SMSLI was introduced where a set of ultra-narrowband spectral line images is collected by a single snapshot under uniform target illumination simultaneously by several spectral lines [9]. For example, standard RGB color cameras can record three spectral line images by a single snapshot if the illumination comprises three discrete spectral lines, each of them positioned within one of the camera's detection bands - R, G or B [10]. Similarly, four-band cameras ensure snapshot detection of four spectral line images, each of them related to one of the illumination wavelengths [11].

Currently, integrated "3 in 1" RGB laser modules emitting simultaneously three spectral lines in the blue, green and red

*) janis.spigulis@lu.lv

regions of visible (VIS) spectrum [12] are market available. They are well-suited for triple spectral line illumination of skin, e.g. by using laser-coupled side emitting optical fiber loop that ensures uniform illumination of the examined skin region [13]. Such design was implemented in a prototype device for triple spectral line whole-body imaging where fast discrimination between large number of pigmented and vascular skin malformations was demonstrated [14]. Continuing this study, the prototype was updated by adding two near-infrared (NIR) imaging channels to reach deeper skin layers and clinically validated to assess the potential of this technology for improved remote detection and early screening of skin cancer.

2. THE PROTOTYPE DEVICE

The developed prototype device shown in Figure1 consists of an illumination module and a high-resolution imaging module. Illumination module enables simultaneous or sequential emission of spectral lines at wavelengths 450 nm, 520 nm and 638 nm from a 3W RGB laser [14] and/or 850 nm from a 4W laser (both from *HangZhou NaKu Technology Co., Ltd*., CN). The lasers are SMA-coupled to two spirals of silica core side-emitting optical fibers with distal end reflectors (*Anda Optec Ltd*., LV) that ensure uniform target illumination at all laser wavelengths; total lengths of the fibers are 60 m and 30 m, respectively. Both fiber spirals are glued to a 3 mm PMMA mirror plate which also serves as a structural holder. Illumination power density at the working distance 70 cm for 450 nm laser line reaches 22 μW/cm^2, for 520 nm – 17 μW/cm^2, for 638 nm –15 μW/cm^2, and for 850 nm – 34 μW/cm^2.

NIR band illumination is additionally provided by two side panels with 940 nm LEDs (SMB1N-940DS-02, *ROITHNER LASERTECHNIK GmbH*, DE) emitting in total 30W. The device incorporates an LED current stabilizer (NLDD-1400H, *MEAN WELL ENTERPRISES CO., LTD.,* TW), capable of providing a constant current of 1400 mA to the LED panels. Each panel contains 15 LEDs connected in series, ensuring the same current flow through every diode. Each LED is mounted on a custom-designed aluminum PCB, attached to a larger aluminum heat sink. This design ensures efficient heat dissipation, maintaining the LED temperature close to ambient levels and preventing overheating or reduction in luminous intensity. LED brightness control is implemented using an Arduino microcontroller. In real measurements, the radiation intensity was adjusted so that the perceived image was neither too bright nor too dark, thus the illumination power density at 940 nm was set not to exceed 0.2 mW/cm^2.

Inside the fiber spirals, a 61-megapixel *Sony Alpha 7R IV* full-frame color camera (6376x9668 pix., 14-bit resolution) with removed infrared-blocking filter is placed. Both the laser-coupled fiber spirals and the camera represent a single unit mounted on a 1-meter linear rail and driven vertically by a stepper motor. Using a remote controller, the height of camera with illumination fibers can be varied between 0.5 m and 1.5 m, which allows non-contact imaging of patient's large skin areas at any location on his/her body. Images are captured and transferred wirelessly to a computer using *Imaging Edge*

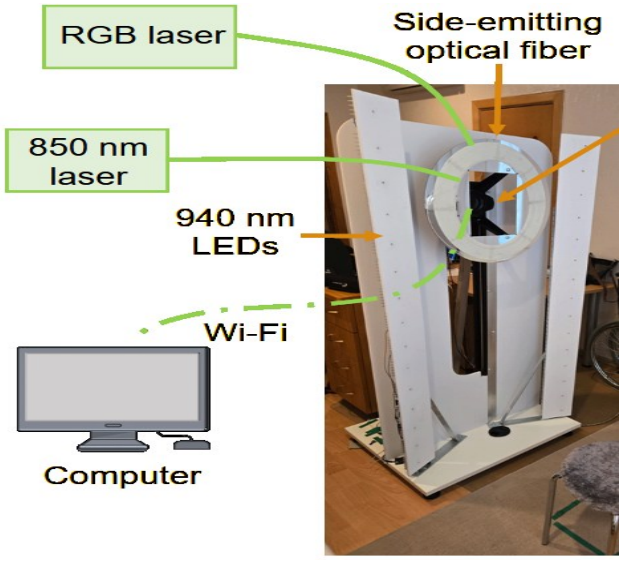

Figure 1. The prototype device for remote multispectral VIS-NIR imaging of full body or large area skin.

Desktop software. Spectral line images of skin are extracted from the camera RGB image data set by the method described in [10]. Unlike the commercial broadband illumination systems, this design provides extremely high spectral selectivity ofimaging at all laser wavelengths (full width at half maximum FWHM < 0.1 nm) and a relatively narrow (FWHM ~ 35 nm) NIR-imaging band centered at 940 nm.

3. THE CLINICAL MEASURMENT PROCEDURE

All clinical measurements were conducted at Oncology Center of Latvia over a period of six months in 2025. The procedure was carried out in full compliance with the World Medical Association Declaration of Helsinki and approved by the ethics committees of Riga East University Hospital (No. AP/08-08.1/25/36) and University of Latvia (No. 13-22/23). A total of 60 patients participated in the study, including 31 women and 29 men, aged between 35 and 93 years. Histologically confirmed clinical diagnoses involved malignant melanoma (MM, n=8, including one lentigo maligna) and basal cell carcinoma (BCC, n=33), along with clinically confirmed BCC, nevi, hemangiomas and seborrheic keratoses, as well as single cases of Bowen's disease and blue nevus. In total, more than 100 color images of different skin lesions were captured and analyzed. Histologically confirmed MM was diagnosed in one woman and seven men of ages 43-81 years. Melanomas were located on the trunk (50%), head and neck (38%), and extremities (13%). Histologically confirmed BCC was diagnosed in 19 women and 14 men of ages 55-93 years, with lesions located on the head and neck (67%), trunk (27%), and extremities (6%).

Images of the patient's skin areas with malformations were captured in a dark room, switching between spectral modalities of illumination sequentially: (i) combined 450/520/638 nm laser lines, (ii) combined 450/520/850 nm laser lines, (iii) each illumination line separately, (iv) 940 nm LED band illumination (the latter two modalities in ~70% of all cases). Patients were positioned approximately 50–70 cm from the lens so that the target skin area was in focus and well illuminated. Calibration images were captured each morning before patient sessions using a white reference (ColorChecker White Balance, *X-Rite*, *Inc*., USA) which was also present during patient imaging. The reference was placed as close to the patient as possible. Depending on the patient's ability to cooperate and maintain the optimal position (considering age, physical condition and lesion location), the entire imaging session typically took less than 20 minutes.

All patient imaging data were anonymized and stored in a dedicated database for further analysis. The data on clinical diagnosis of the skin lesion and a brief medical history of the diagnosis (if available), as well as the participant's name, surname, age and gender were collected. To ensure the protection of participants' personal data, pseudonymization was applied after inclusion in the study and after obtaining informed consent. In the photographs, the patient's face was partially covered by laser protective glasses, and other identifiable body parts (e.g., specific tattoos or features) were also obscured. Additionally, before image processing, the participant's face and intimate areas were blurred.

4. PROCESSING OF SPECTRAL IMAGES

The spectral images of large skin areas were extracted from the camera RGB image data by a custom-developed software (Matlab *R2021b*) as illustrated in Figure 2. Spectral image set related to the above-mentioned illumination wavelength combinations was calculated using the registered RAW images of the white reference and skin. Initially, four spectral line images (450 nm, 520 nm, 638 nm, 850 nm) were considered. In the case of triple visible line illumination, the spectral line intensities I_{450} , I_{520} , I_{638} at each image pixel were found by solving the matrix equation:

$$\begin{bmatrix} I_R \\ I_G \\ I_B \end{bmatrix} = \begin{bmatrix} 1 & 0.039 & 0 \\ 0 & 0.721 & 0 \\ 0.003 & 0.083 & 0.579 \end{bmatrix} \begin{bmatrix} I_{638} \\ I_{520} \\ I_{450} \end{bmatrix} \quad (1),$$

where I_R, I_G and I_B are the mean pixel values of the selected skin area, detected by the camera R, G or B-channel when the 450 nm, 520 nm and 638 nm lasers were switched on. Similarly, at simultaneous blue-green-NIR laser line illumination the intensities I_{450} , I_{520} and I_{850} were found by solving the equation:

$$\begin{bmatrix} I_R \\ I_G \\ I_B \end{bmatrix} = \begin{bmatrix} 1 & 0.054 & 0 \\ 0.350 & 0.993 & 0 \\ 0.670 & 0.115 & 0.798 \end{bmatrix} \begin{bmatrix} I_{850} \\ I_{520} \\ I_{450} \end{bmatrix} \quad (2)$$

where I_R is the detected R-channel signal at 850 nm laser illumination. The numerical values in matrices represent camera RGB pixel outputs of the white reference snapshots taken under the corresponding wavelength laser line illumination [15].

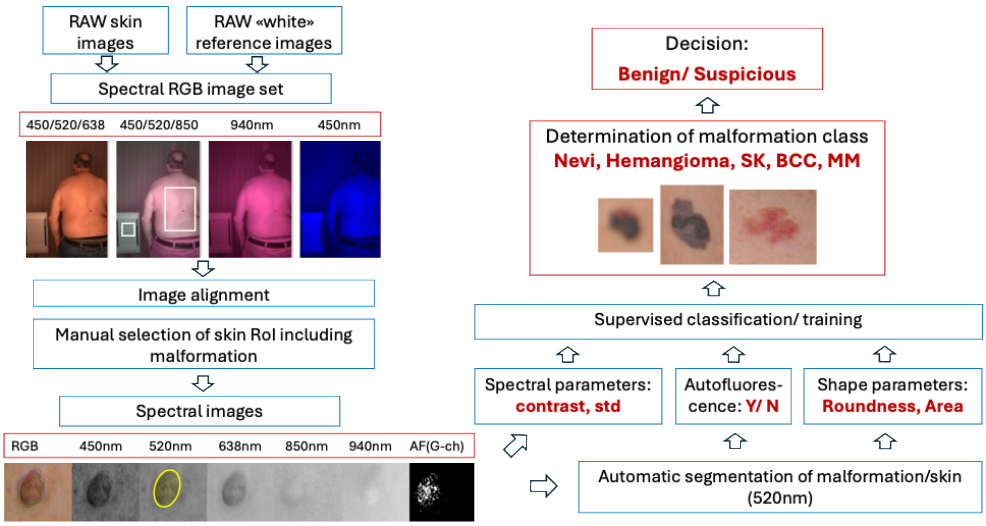

Figure 2. The scheme for obtaining and analysis of the skin malformation's spectral images.

Additionally, the 940 nm band spectral image of skin taken under the NIR LED illumination and recorded in camera's R-channel was analyzed, as well as the 450 nm excited skin autofluorescence binary image from camera's G-channel were obtained for identifying the fluorescing seborrheic keratoses [16]. To compensate image shifts due to patient's body motions, alignment among multiple image sets were performed (Matlab *fitgeotrans* and *imwarp* functions). Then the rectangular region of interest (RoI) was manually set to include the malformation and the surrounding healthy skin.

Next, automatic segmentation of the malformation images was performed to separate the malformation from the surrounding healthy skin. To calculate segmentation mask, we used Otsu's method [17] applied to 520 nm RoI image. This binary mask was used for all spectral images to calculate several specific parameters with eventual diagnostic potential.

Malformation's shape-related parameters - area A and roundness R - were calculated by *Matlab* image property measurement *regionprops* function:

$$A = \sum pixels_{malf} \quad (3),$$

$$R = 4\pi A/P^2 \quad (4),$$

where P – perimeter of the malformation.

Spectral parameters were calculated from the detected pixel intensities of malformation and the surrounding healthy skin. We analyzed the following parameters:

- I_{malf} – normalized pixel's intensity distribution inside the malformation (values from 0 to 1),
- $\overline{I_{malf}}$ – median intensity of the malformation pixels (520 nm mask),
- $\overline{I_{skin}}$ – median intensity of the surrounding healthy skin pixels (520 nm mask).,
- Contrast – $C = \overline{I_{skin}} / \overline{I_{malf}}$,
- Relative standard deviation of malformation pixels – $Std_{malf} = std(I_{malf})/\overline{I_{malf}}$,
- Relative standard deviation of healthy skin pixels – $Std_{skin} = std(I_{skin})/\overline{I_{skin}}$,
- Autofluorescence at 450 nm excitation, detected in G channel of camera (false/true):

$$AF = \begin{cases} 0, if\ I_{G\_malf} < 2^{-14} \\ 1, if\ I_{G\_malf} > 2^{-14} \end{cases} \quad (5),$$

- Empiric parameters p_{450} and p_{520}:

$$p_{450} = \frac{C_{638} \cdot C_{850}}{C_{450}} \quad (6),$$

$$p_{520} = \frac{C_{638} \cdot C_{850}}{C_{520}} \quad (7).$$

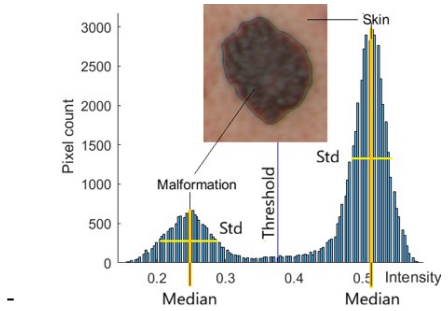

Figure 3. An example of spectral image histogram and its standard deviations (skin + malformation) .

The AF parameter was calculated from camera's G-channel data when the image was taken under single 450 nm spectral line illumination. As the AF signal was relatively weak, the sensitivity of autofluorescence detection critically depended on camera bit depth. The *Sony Alpha* camera matrix has 14-bit resolution, so the theoretical limit of detected AF intensity is $1/2^{14}$, which defines the minimum threshold for AF signal. The two empiric parameters p (calculated for each image pixel) are comparable to the melanoma-sensitive parameter proposed in [18], but with slightly different working wavelength values. Both standard deviations (Std) were calculated from the image histograms – distribution functions of image pixels with equal output intensities (see Figure 3).

Five classes of skin malformations were selected for further analysis: pigmented nevi - 62 cases, hemangiomas - 18 cases, seborrheic keratoses - 27 cases, basal cell carcinomas - 33 cases, and melanomas - 7 cases. Both malignant malformations included also ulcerated ones. Single lesions such as Bowen's disease, lentigo maligna and blue nevus were excluded from further analysis.

To explore the future potential of skin malformation's automatic classification using AI approaches, the machine learning algorithm (Matlab *classificationLearner*) was tested: each input in the training dataset of above-regarded parameters was paired with a corresponding output label – the group of malformations. The model was trained with a validation scheme, to protect against overfitting by applying cross-validation. For reaching this, the data were set to 5 folds and the accuracy for each fold estimated. For data validation, linear discriminant model (LDA) was chosen.

5. RESULTS

Concerning the NIR images of skin malformations - a novelty for this prototype system, no essential differences between the 850 nm and 940 nm skin spectral images were observed, so further only 850 nm images will represent the NIR spectral range. The most interesting feature for spectral images of large skin areas comprising numerous pigmented lesions (including malignant) was the observed "fading" effect: nearly all benign lesions recorded in the visible spectral images

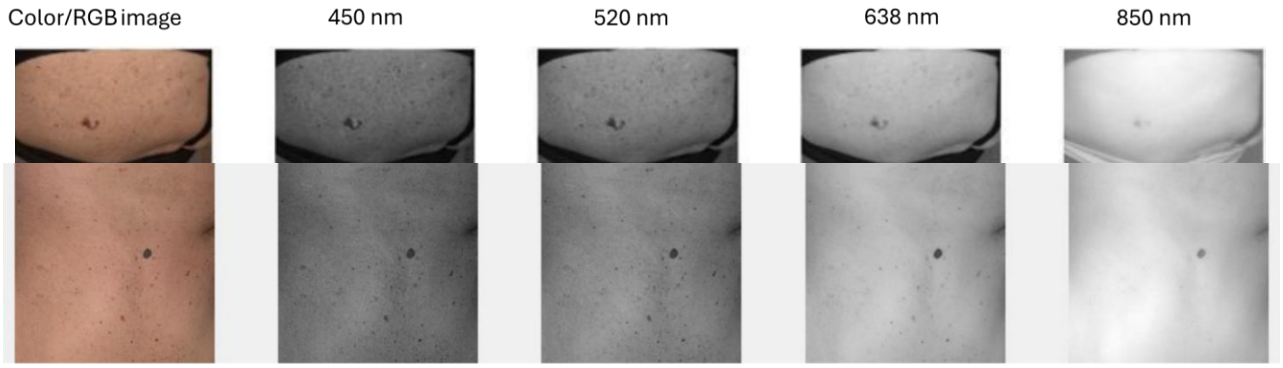

Figure 4. Comparison of the recorded spectral line images for two cases of melanomas surrounded by nevi and sun damaged skin on patient's back. Only melanomas remained visible in the 850 nm spectral image (the "NIR-fading" effect).

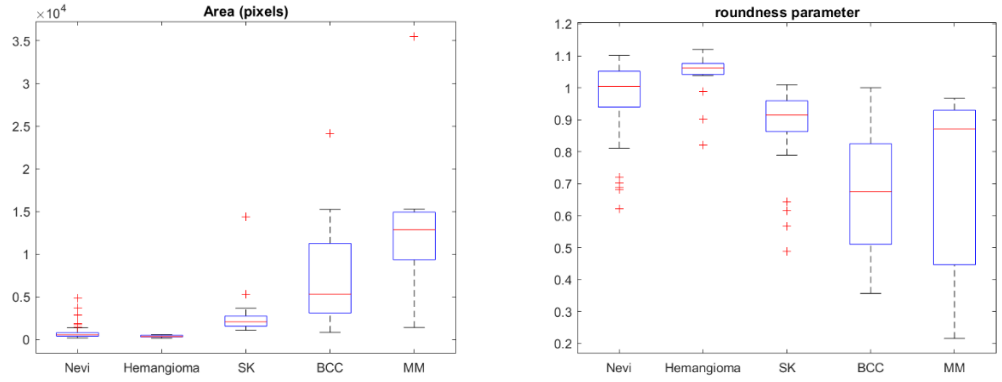

Figure 5. Comparison of the areas (number of pixels) and the roundness parameters for five classes of skin malformations.

faded with wavelength and fully disappeared in the NIR image, while the melanomas remained clearly visible, as illustrated in Figure 4. It is also related to the ulcerated basal cell carcinomas.

However, some benign lesions were recorded in the 850 nm spectral images, as well – namely, hemangiomas (due to higher absorption of hemoglobin in NIR) and a few keratoses and nevi (could be related to their thickness and increased melanin content, respectively). To distinguish them from the malignant melanoma and basal cell carcinoma, one or more of the above-listed parameters can be exploited.

In Figure 5, the segmented areas and roundness parameters for five selected classes of the examined malformations are compared. In both cases melanomas and basal cell carcinomas convincingly stand out. A more objective criterion appears to be the roundness of malformation where values below 0.8 characterize a malignant formation.

To separate melanomas and basal cell carcinomas, the contrast in the 850 nm spectral images of the malformations with roundness less than 0.8 can be considered. In Figure 6, contrasts of the five classes of malformations in the green (520 nm) and NIR (850 nm) spectral line images are compared. If the contrasts in visible images are mutually comparable, they are clearly different in the NIR-images – melanomas exhibit the contrast values >1.1 while basal cell carcinomas along with other NIR-detected malformations are characterized by the contrast values below 1.1.

Another option to distinguish between melanomas and basal cell carcinomas (both with roundness parameters below 0.8) is comparing the standard deviation (Std) values of their spectral image pixels. As an example, in Figure 7 the Std data for 520 nm and 850 nm spectral images of all regarded malformations are presented. Again, in the green images the Std values mainly overlap, while in the NIR-images melanomas clearly stand out (Std > 0.06).

An additional criterion to sort-out seborrheic keratoses - formations sometimes visually misclassified as malignances, the 450 nm excited autofluorescence from the malformation region with intensity higher than that of the surrounding healthy skin can be used as a marker - the other regarded groups of skin malformations lack this property [16].

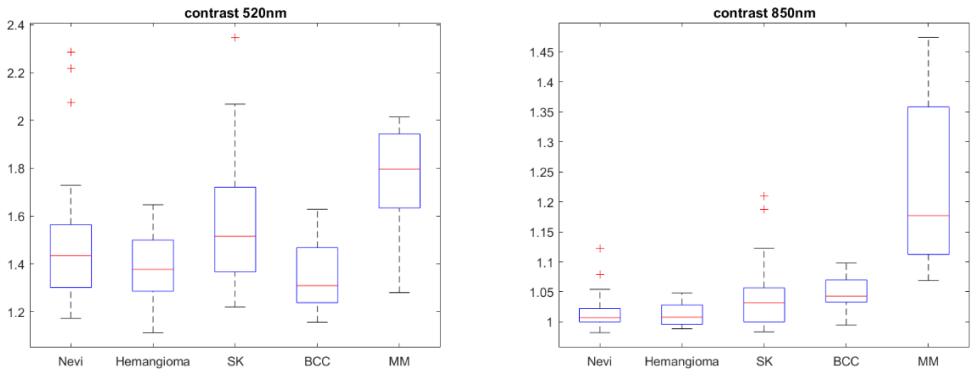

Figure 6. Comparison of the contrast values in skin malformation spectral line images at 520 nm (left) and 850 nm (right).

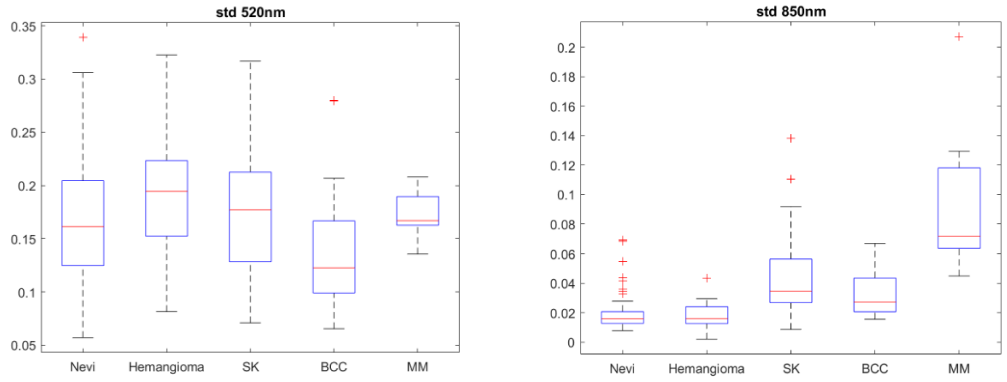

Figure 7. Comparison of the standard deviation values calculated from the malformation's spectral image pixel histograms at 520 nm (left) and 850 nm (right).

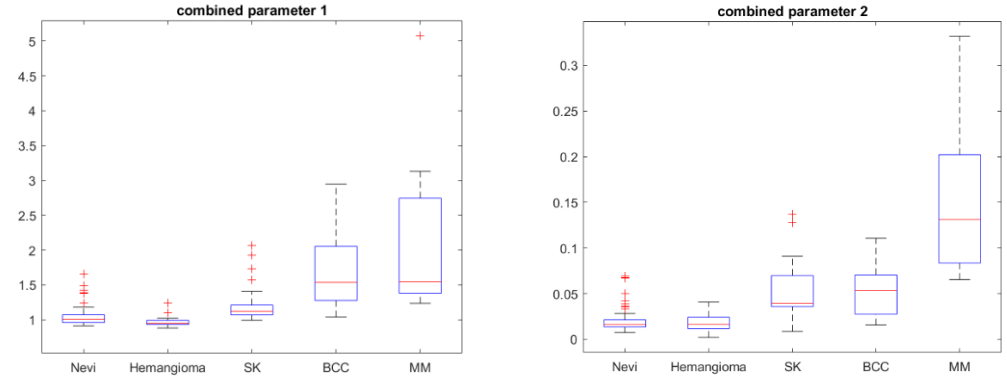

Figure 8. Combined parameters C_{850}/R (left) and Std_{850}/R (right) calculated for five classes of malformations.

Specific combined parameters yielded from the NIR spectral line images of malformations, e.g. the NIR contrast–to-roundness ratio or NIR Std–to-roundness ratio, also are potentially useful for fast selection of skin malignances, see Figure 8. The C_{850}/R ratio separates benign and malignant formations while the Std_{850}/R ratio helps distinguishing between MM and BCC.

Along with data extracted from spectral images captured under the 450 nm, 520 nm and 850 nm combined illumination (available by a single snapshot), also those related to the red laser line 638 nm can be exploited as additional melanoma markers. Figure 9 shows the values of empiric parameter *p* calculated for all five pathology groups using the 450/638/850

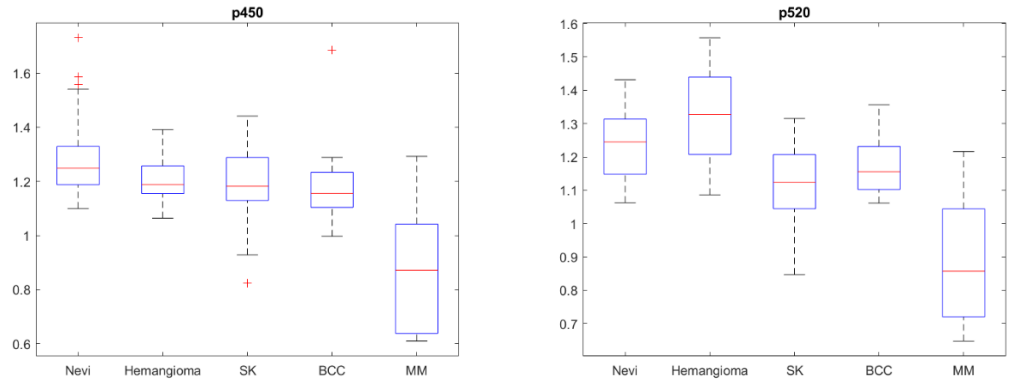

Figure 9. Values of the melanoma-specific parameter *p* at imaging wavelength combinations 450/638/850 nm (left) and 520/638/850 nm (right) for five classes of skin malformations.

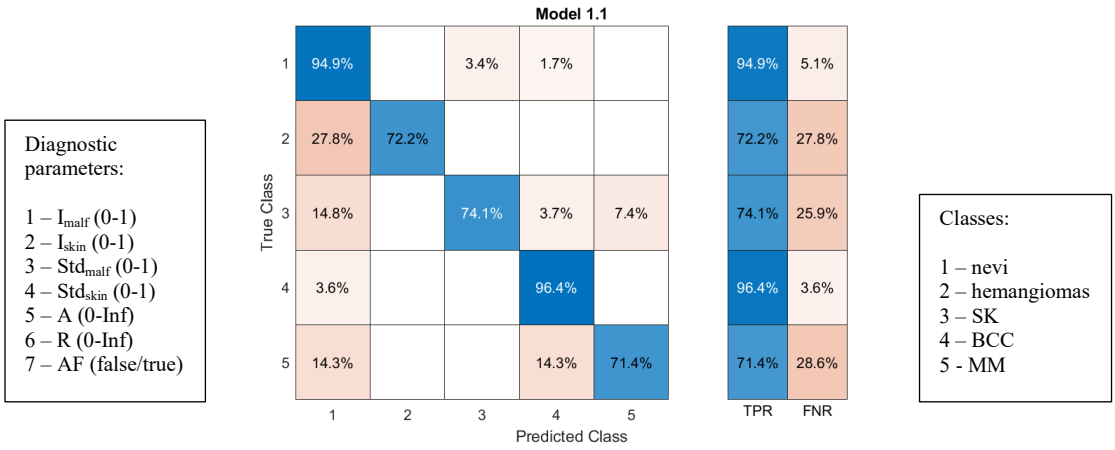

Figure 10. Results of the AI-based automatic classification of skin malformations using seven specific spectral image parameter sets taken at 450 nm, 520 nm, 638 nm, and 850 nm (in total 19 parameters).

nm and 520/638/850 nm imaging wavelengths sets. In both cases the *p*-values for melanomas are well-separated from those of the other examined skin malformations. This evaluation needs two snapshots (e.g. at the 450/638 nm and 450/850 nm combined illumination), as both 638 nm and 850 nm images are extracted from the camera R-channel.

Finally, Figure 10 presents the results of AI-based calculations, testing the ability of AI for automatic malformation's classification based on 19 selected parameters of the spectral line images collected in this study. One can see that the AI-prediction rate is relatively high, reaching the true positive values in the range 71-96 %. As expected, the lower is number of used samples, the lower is AI precision – that is why the calculated TPR for melanoma (n=7) is the lowest.

6. DISCUSSION

This proof-of-concept study was mainly aimed at exploring the clinical potential of remote skin cancer detection and screening by combined visible/near-infrared multispectral imaging. Some of the main outcomes and conclusions can be highlighted:

- Malignant skin malformations (melanomas, basal cell carcinomas), due to their deeper invasion, are well-exposed in the NIR spectral images (850 nm, 940 nm), while most benign lesions that are clearly visible in the blue, green and red images, disappear in the NIR images of skin (the "NIR-fading" effect).
- Both melanomas and basal cell carcinomas have notably lower roundness (< 0.8) than the benign lesions in visible images, which enables fast sorting of malignancies; to separate melanomas from basal cell carcinomas, differences in parameters of their NIR spectral images (e.g. contrast and/or pixel standard deviation) can be exploited.
- Single snapshot visible-NIR multispectral imaging (e.g. at 450/520/850 nm combined illumination) can be recommended for fast remote screening of skin cancer, based on extracted melanoma-sensitive clinical criteria like C_{850}/R - the ratio of NIR image contrast to the roundness of malformation.
- Empiric spectral criteria like p_{450} and p_{520}, obtainable by the double snapshot RGB technique, are also helpful for fast detection of skin cancers.
- Suitability of the developed equipment and software for fast contactless whole-body skin cancer detection and/or screening has been demonstrated. Still, much simpler equipment design also could be useful for routine clinical applications – e.g. as a portable device with high resolution black-and-white camera and fast sequential multi-LED illumination comprising blue, green, red and near infrared spectral bands.
- Development of advanced software ensuring fast extraction of the VIS-NIR spectral images of skin malformations and calculation of appropriate malignancy criteria immediately after the imaging procedure, still in the presence of patient in the doctor's office, is a future challenge.
- Artificial intelligence approaches for skin cancer detection using VIS-NIR multispectral images are promising; however, a larger collection of clinical spectral images would be needed to train AI systems effectively.

7. SUMMARY

The developed prototype system for visible and near-infrared remote multispectral imaging of skin malformations with high spectral selectivity and its clinical validation on 60 patients have highlighted new prospects in fast remote screening of skin cancer. Several cancer-sensitive clinical criteria, extracted from the VIS-NIR spectral images of skin malformations, have been proposed. The future work involves development of a portable device for remote VIS-NIR multispectral skin imaging with software enabling fast extraction of the cancer-sensitive criteria from the multispectral image data.

8. ACKNOWLEDGEMENTS

This research was funded by the Recovery and Resilience Facility project "Internal and External Consolidation of the University of Latvia" (No. 5.2.1.1.i.0/2/24/I/CFLA/007), grant No. LU-BA-PA-2024/1-0006.

REFERENCES

1. Korotkov K., Quintana J., Campos R., Jesús-Silva A., Iglesias P., Puig S., Malvehy J., Garcia R., "An improved skin lesion matching scheme in total body photography", *IEEE J. Biomed. Health Inform.,* **23**, 586–598 (2019). doi: 10.1109/JBHI.2018.2855409.
2. "VECTRA 3D Whole body 3D imaging system", *Canfield*, https://www.canfieldsci.com/imaging-systems/vectra-wb360-imaging-system, last accessed 16.12.2025.
3. "State-of-the-art technology for dermatology and aesthetics", *FotoFinder*, https://www.fotofinder.de/en/technology, last accessed 16.12.2025.
4. Goessinger E.V., Dittrich P.G., Nöcker P., Notni G., Weber S., Cerminara S., Muhleisen B., Navarini A.A., Mau L.M., "Classification of melanocytic lesions using direct illumination multispectral imaging", *Sci.Rep.,* **14**, 19036 (2024). https://doi.org/10.1038/s41598-024-69773-x.
5. Sultana A.E., Oniga M., Rus P.F., Dobre A.L., Orzan O.A., "MelanoDet: multimodal imaging system for screening and analysis of cutaneous melanoma," *IEEE Access*, **13**, pp. 61469-61482 (2025). doi: 10.1109/ACCESS.2025.3557628.
6. Aggarwai P., Papay F.A., "Applications of multispectral and hyperspectral imaging in dermatology", *Experim.Dermatol.,* **31**(8), 1128-1135 (2022). https://doi.org/10.1111/exd.14624
7. Rey-Barroso L., Peña-Gutiérrez S., Yáñez C., Burgos-Fernández F.J., Vilaseca M., Royo S., "Optical technologies for the improvement of skin cancer diagnosis: a review", *Sensors,* **21**(1), 252 (2021). https://doi.org/10.3390/s21010252.
8. Bozsányi S., Varga N., Farkas K., Hamilton-Meikle P., Banvolgyi A., Lihacova I., Lihachev A., Skrastina M., Paragh G, Wikonkal N., Medvecz M., Kiss, N., "Comparison of the effectiveness of optically guided high-frequency ultrasound and multispectral imaging for the in vivo measurement of melanoma tumor thickness", *J.Investig.Dermatol.,* **143,** S86. (2023). doi: 10.1016/j.jid.2023.03.507.
9. Spigulis J., "Ultra-Narrowband Multispectral Imaging: Techniques and Applications", *CRC Press*, Boca Raton (FL), 97 p. (2024). ISBN 9781032757292.
10. Spigulis J., Elste L., "Single-snapshot RGB multispectral imaging at fixed wavelengths: proof of concept", *Proc. SPIE* **8937**, 89370L (2014). https://doi.org/10.1117/12.2039442.
11. Spigulis J., Rupenheits Z., Rubins U., Mileiko M., Oshina I., "Spectral line reflectance and fluorescence imaging device for skin diagnostics", *Appl. Sci.*, **10**, 7472 (2020). https://doi.org/10.3390/app10217472.
12. "Principle and application of RGB laser module", https://www.loshield.com/news/principle-and-application-of-rgb-laser-module-84962108.html, last accessed 16.12.2025.
13. Patent LV 15491 B, 2020. Device for uniform surface illumination simultaneously by several laser spectral lines.
14. Spigulis J., Rubins U., Kviesis-Kipge E, Saknite I., Oshina I., Vasilisina E., "Triple spectral line imaging of whole-body human skin: equipment, image processing, and clinical data", *Sensors*, **24**, 7348 (2024). doi:10.3390/s24227348.
15. Patent LV 15705 B, 2023. Method and device for determination of photo-camera relative spectral sensitivities at fixed wavelengths.
16. Lihachev A., Lihacova l., Plorina E.V., Lange M., Derjabo A., Spigulis J., "Differentiation of seborrheic keratosis from basal cell carcinoma, nevi and melanoma by RGB autofluorescence imaging", *Biomed.Opt.Expr.,* **9**(4),1852-1858 (2018). doi: 10.1364/BOE.9.001852.
17. Otsu, N., "A threshold selection method from gray-level histograms", *IEEE Trans.Syst.,Man, Cybern*., 9(1), 62–66 (1979). doi: 10.1109/TSMC.1979.4310076.
18. Diebele I., Kuzmina I., Lihachev A., Kapostinsh J., Derjabo A., Valaine L., Spigulis J., "Clinical evaluation of melanomas and common nevi by spectral imaging", *Biomed.Opt.Expr.,* **3**(3), 467-472 (2012). doi: 10.1364/BOE.3.000467.